05FTM05

Computerized Design of Face Hobbed Hypoid Gears: Tooth Surfaces Generation, Contact Analysis and Stress Calculation

by: M. Vimercati, Politecnico di Milano and A. Piazza, Centro Ricerche FIAT – ScpA

American Gear Manufacturers Association

TECHNICAL PAPER

Computerized Design of Face Hobbed Hypoid Gears: Tooth Surface Generation, Contact Analysis and Stress Calculation

Martino Vimercati, Politecnico di Milano and Andrea Piazza, Centro Ricerche FIAT – ScpA

Abstract

While face milled hypoid gears have been widely studied, about face hobbed ones only very few studies have been developed. Aim of this paper is just to propose an accurate tool for computerized design of face hobbed hypoid gears. Firstly, a mathematical model able to compute detailed gear tooth surface representation will be derived; then, the obtained surfaces will be employed as input for an advanced contact solver that, using a hybrid method combining finite element technique with semianalytical solutions, is able to efficiently carry out contact analysis under light and heavy loads and stress calculation of these gears.

American Gear Manufacturers Association
500 Montgomery Street, Suite 350
Alexandria, Virginia, 22314

October, 2005

ISBN: 1-55589-853-X

Computerized Design of Face Hobbed Hypoid Gears: Tooth Surfaces Generation, Contact Analysis and Stress Calculation

M. Vimercati [a], A. Piazza [b]
[a] Politecnico di Milano – Dipartimento di Meccanica, Italy, e-mail: martino.vimercati@polimi.it
[b] Centro Ricerche FIAT – ScpA, Italy, e-mail: andrea.piazza@crf.it

Nomenclature

N_b	Number of blade groups
R_b	Ratio between N_b and the number of being generated gear teeth
r_b	Blade Radius
ε_b	Eccentric Angle
Γ_b	Hook Angle
h_f	Blade Height
κ_e	Rake Angle
α_e	Blade Angle
r_e	Edge Radius
L_T	Length of Toprem®
τ	Angle of Toprem®
ρ_t	Blade radius of curvature
i	Tilt Angle
j	Swivel Angle
S_r	Radial Setting
q	Cradle Angle
E_m	Blank Offset
γ_m	Machine Root Angle
ΔX_p	Machine Center to Back
ΔX_b	Sliding Base
R_a	Ratio of Roll

1. Introduction

In the geared transmission design it is very useful to have a numerical tool able to simulate the real behavior of the gear drive, searching for proper contact pattern, low level of transmission error and acceptable fillet stress. In this paper a set of numerical procedure for performance analysis of face hobbed hypoid gear will be proposed.

As well known, this kind of gear is largely applied when it is needed to transfer power and motion between intersecting and crossing axles [1]. Hypoid pairs are mainly manufactured by face hobbing (FH) or face milling (FM) cutting process [2]; while this latter uses a single indexing cutting method, in FH process the being generated gear has continuous rotation and rotates in a timed relationship with the cutter. As the gear is being cut, successive cutter blades groups engage successive tooth slots guaranteeing a continuous indexing. This process is now spreading in automotive industry because of its fast manufacturing time.

Since many decades, a lot of studies about tooth surface representation, contact and stress analysis of FM gears have been carried out [3-6]. On the contrary, about FH process, which is considerably more complex, only a small number of papers have been published. Regarding tooth geometry, Litvin et al. derived a mathematical model able to describe tooth surfaces only of a non-generated Oerlikon gear member [7]; Fong proposed a computerized universal generator able to simulate virtually all primary spiral bevel and hypoid cutting methods without providing a detailed description of the FH case [8]. Referring to performance analysis, the state of art is even worse: in the open literature any work has been found. Consequently, nowadays, it is possible to study this kind of gears only by using, basically as a “black box”, proprietary software which has been developed by manufacturing machine and tools suppliers.

Goal of this paper is just to propose an integrated tool for computerized design of FH hypoid gears.

The first step in order to build a reliable numerical model is to get a fine geometrical representation of gear tooth surfaces. With this aim, a series of algorithms able to compute tooth surfaces of FH gears starting from cutting process will be described [9]. The geometry of real FH head cutter (Gleason Tri-Ac®) will be firstly analyzed; many kinds of blade configuration (straight and curve blades, with or without Toprem®) will be considered. Then, according to the theory of gearing, FH cutting process (with and without generation motion) will be simulated and gear tooth surfaces equations will be computed. The proposed mathematical model is able to provide an accurate description of the whole tooth, including fillet region; it will also take into account undercutting occurrence, which is very common in FH gears due to uniform depth tooth [4]. By means of this model, tooth surfaces of a real gear drive, which is mounted in a truck differential system, will be computed and the results will be validated by comparing them with the ones calculated by a reference proprietary software and with the real surfaces.

Then, the obtained tooth surfaces will be used as fundamental input for a powerful contact solver which is based on a unique semianalytical finite element formulation [10-11]. Firstly, the gear drive it will study under light load by monitoring, for drive and coast side, the contact pattern and transmission error (Tooth Contact Analysis - TCA). After that, with the aim to find out gear drive performance in the real service conditions, a set of torque values will be applied and the influence of the load on contact pattern, on transmission error and on load sharing will be accurately analyzed (Loaded Tooth Contact Analysis - LTCA). Contact pressure and stress distribution will be also evaluated. The obtained results will be compared with the ones calculated by a reference software.

2. Theoretical Background of Face Hobbing Method

As known [2], FH head cutter is provided with a proper number of blade groups N_b, each of them consists in an outer and an inner blade. As reported in Figure 1, in order to accomplish continuous indexing, the head cutter and the being generated gear are rotating in opposite directions and the next group of blades will start to cut the next gear tooth after that the current group of blades has finished cutting the current tooth.

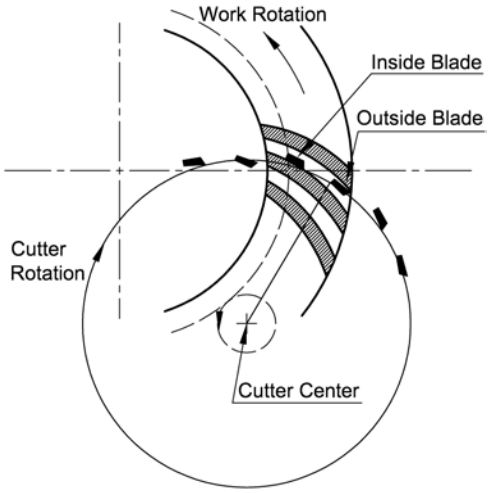

Figure 1. Sketch of FH cutting process

In this way, the angular velocity of the head cutter ω_b is related to the angular velocity of the work-piece ω_w according to the ratio between the number of blade groups N_b and the number of being generated gear teeth N_w:

$$R_b = \frac{N_b}{N_w} = \frac{\omega_w}{\omega_b} \quad (1)$$

It is evident that the edge of the blade, during cutting, tracks an epicycloid curve. In order to accommodate this path, unlike FM method, the effective cutting direction of the blade is not perpendicular to the cutter radius and the blade is moved in the head cutter tangentially to an offset position.

Fig. is referred to the non-generated process (Formate®); if a generated tooth is needed, the generation motion, which relates cradle and work-piece rotation, has to be superimposed.

Traditionally, FH gear drive has uniform depth tooth; it follows that FH tooth often shows undercut toe-section with sharp topland. This latter inconvenient can be eliminated by introducing a secondary face angle; undercutting avoidance could be a difficult task and often FH gear drives work affected by it [2, 12].

3. Simulation of Face Hobbing Cutting Process: Tooth Surface Generation

According to the theory of gearing [3-4, 13], in order to get the analytical representation of gear tooth surfaces, firstly cutting process (i.e. head cutter, cutting blades and cutting machine) has to be described. It will be clear that [9], due to the complexity of FH cutting process, FH cutting blades require a more complicated representation than the ones usually illustrated in the literature (typically for FM method). In this paper a real FH process, Gleason Tri-Ac®, will be studied.

3.1. Cutting Tools: Head Cutter and Cutting Blades

As shown (Figure 1), FH head cutter carries a given number N_b of blade groups; each group contains an outer blade (OB) for cutting concave gear side and an inner one (IB) for convex side. Figure 2 reports, from two different viewing points, one blade group in a Gleason Tri-ac® head cutter.

Referring, for example, to the outer blade, in order to correctly locate the blade in the head cutter, the pitch point P of cutting edge (see also Figure 3) has to be defined. The distance from this point to the head cutter center is the equal to r_b; the angle ε_b is introduced in order to take into account that FH process, unlike FM, shows blades that are not aligned to the cutter radius. It is also evident that the blade is not perpendicular to the head cutter plane, but it is mounted at an angle Γ_b with respect to the head cutter rotation axis. The distance from the pitch point P to the tip of the blade is measured by h_f.

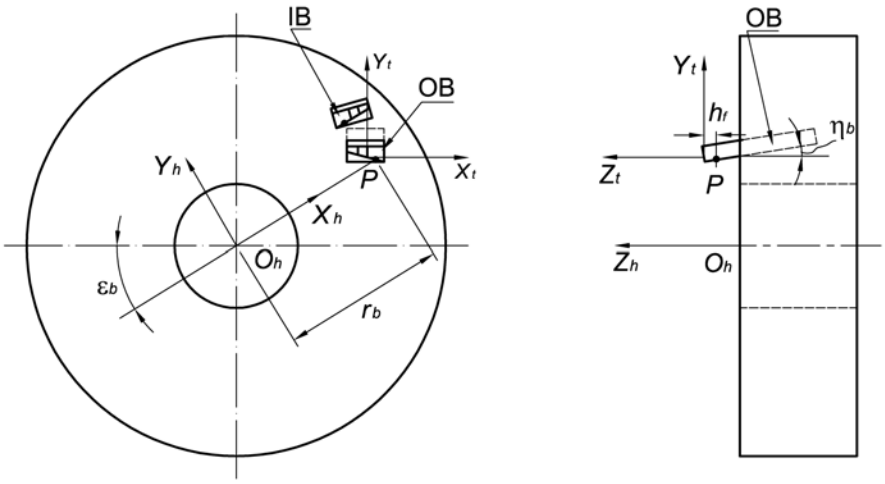

Figure 2. Sketch of a blade group mounted in the FH head cutter.

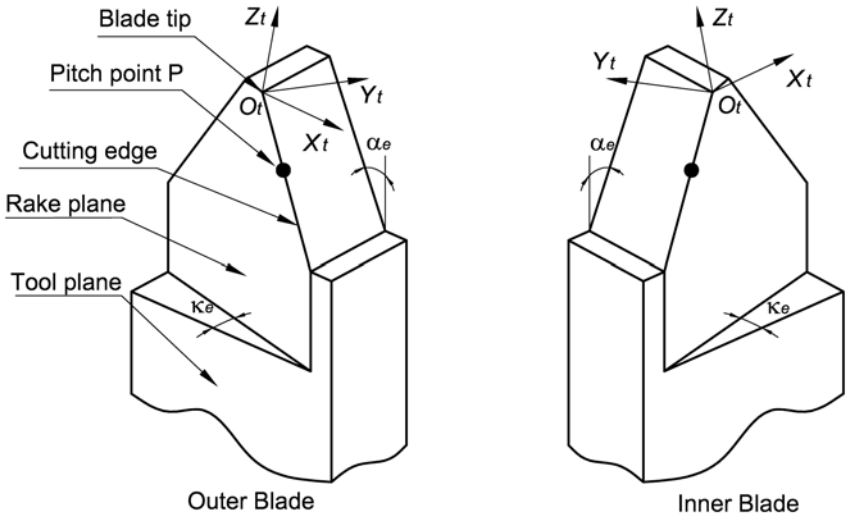

Figure 3. Details of the FH blades.

Figure 3 shows the details of outer and inner blades. It is evident that the cutting edge lies entirely on a plane, called Rake plane, which forms an angle κ_e with tool plane. It is also introduced the angle α_e as the angle between the vertical axis of the blade and the projection of the cutting edge on the tool plane.

Once the blade geometry has been introduced, it is possible to compute the analytical formulation of the cutting edge. Many blade profiles are available in commerce. In this paper, a complex blade shape - curved with Toprem® - will be analyzed; simpler configurations as straight blade with and without Toprem® or curved blade without Toprem® can be easily derived starting from the following discussion. The particular disposition of the cutting edge on the Rake plane requires to set up the reference frame S_t (Figure 2 and 3) and to search firstly for the analytical description of projection on X_tZ_t plane of the cutting edge. Figure 4 shows the projection on this plane of a curved blade with Toprem®; the following sections, which are function of the curvilinear coordinate s, have been defined:

I) Bottom: straight horizontal segment;

II) Fillet: circular arc of radius r_e and center at point R (x_R, z_R);

III) Toprem®: inclined straight segment characterized by the length L_T and the angle τ;

IV) Curved blade: circular arc with radius of curvature ρ_t and center at point O (x_O, z_O). At pitch point P the segment tangent to the blade is inclined by an angle equal to α_t.

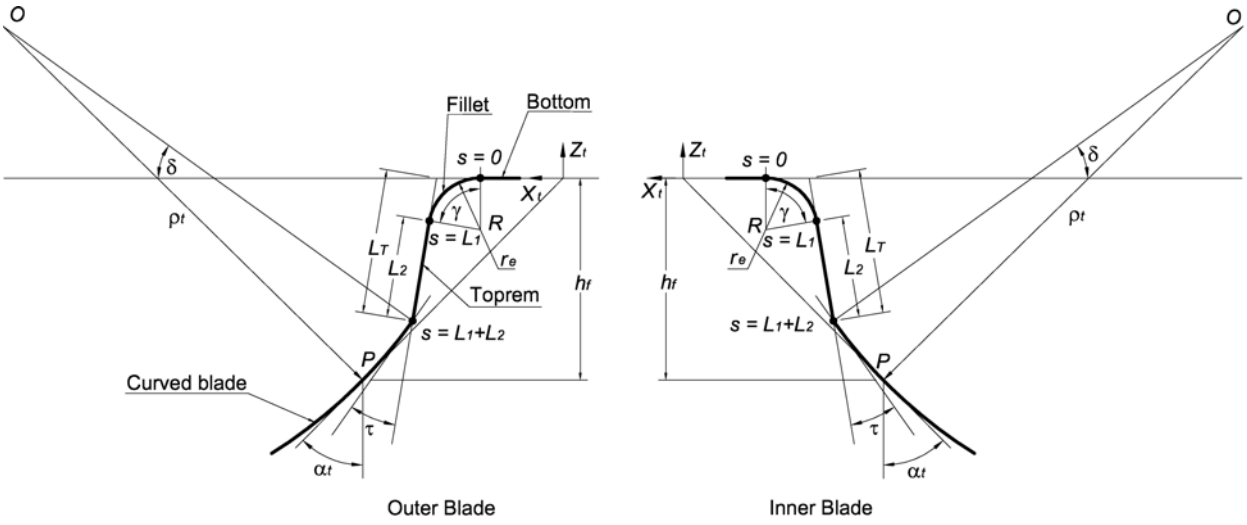

Figure 4. Projection on X_tZ_t plane of curved blades with Toprem®.

The analytical representation of the blade profile has been computed as follows:

for $s \le 0$

$$\begin{Bmatrix} x_t(s) \\ z_t(s) \end{Bmatrix} = \begin{Bmatrix} \pm s + x_R \\ 0 \end{Bmatrix} \tag{2.a}$$

for $0 < s \le L_1$

$$\begin{Bmatrix} x_t(s) \\ z_t(s) \end{Bmatrix} = \begin{Bmatrix} x_R \pm r_e \sin(s / r_e) \\ -r_e(1-\cos(s / r_e)) \end{Bmatrix} \tag{2.b}$$

for $L_1 < s \le L_1 + L_2$

$$\begin{Bmatrix} x_t(s) \\ z_t(s) \end{Bmatrix} = \begin{Bmatrix} x_R \pm r_e \sin(\gamma) \pm (s - L_1)\sin(\delta - \tau) \\ -r_e(1-\cos(\gamma)) - (s - L_1)\cos(\delta - \tau) \end{Bmatrix} \tag{2.c}$$

for $L_1 + L_2 < s$

$$\begin{Bmatrix} x_t(s) \\ z_t(s) \end{Bmatrix} = \begin{Bmatrix} x_O \mp \rho_t \cos(\delta + (s - L_1 - L_2)/\rho_t) \\ z_O - \rho_t \sin(\delta + (s - L_1 - L_2)/\rho_t) \end{Bmatrix} \tag{2.d}$$

The value of the parameters r_e, L_T, τ and ρ_t depends upon the chosen cutter blades. In order to calculate (x_R, z_R), (x_O, z_O), δ, L_1 and L_2 it is necessary to develop some simply geometrical considerations based on Figure 4; the value of the angle α_t is derived from α_e.

Blade profile y_t component is computed by imposing that an arbitrary point of the blade $\boldsymbol{r}_t(s) = [x_t(s), y_t(s), z_t(s)]$ and the blade tip O_t [0,0,0] lie on the Rake plane.

Starting from vector $\boldsymbol{r}_t(s)$, by means of some coordinates transformations, it is useful to measure the blade profile also in the head cutter reference frame S_h (Fig. 2), obtaining vector $\boldsymbol{r}_h(s)$. This latter representation will be the starting point for computation of tooth surfaces equations.

3.2. Cutting Process and Tooth Surface Generation

In order to numerically compute gear tooth surfaces, the classic theory of gearing requires to compute a proper set of coordinate transformations able to simulate cutting process and to represent the cutting edge in reference frame of being generated gear [13].

Consider Fig. 5, where a FH cutting machine set up to cut a generated pinion is shown. In order to describe the machine settings, a set of reference frames have to be introduced. Firstly, the system S_m, which is fixed and rigidly connected to the cutting machine, is defined; it has the origin O_m in the center of cradle and Z_m axis coinciding with the cradle rotation axis. Then, reference frame S_h, which has been introduced in the previous section for blade profile computation, is considered; it allows to measures the head cutter rotation θ and to take into account the tilt and swivel angles. The origin O_h is located by means of the distance S_r and the angle q. Finally, system S_w, which is rigidly connected to the work-piece, is introduced; its origin O_w is placed using the following blank settings: E_m, γ_m, ΔX_p and ΔX_b. Z_w axis is coinciding with the gear rotation axis. In order to accomplish the peculiarity of FH process (i.e. continuous indexing), the system S_w has to rotate about Z_w axis by an angle equal to $R_b\theta$ (see Eq. (1)). If, as in this case, a generated tooth is needed, it is necessary to add to the work-piece rotation a term equal to $R_a\phi$ where R_a is the ratio of roll and ϕ is the cradle rotation angle (i.e. of the system S_c).

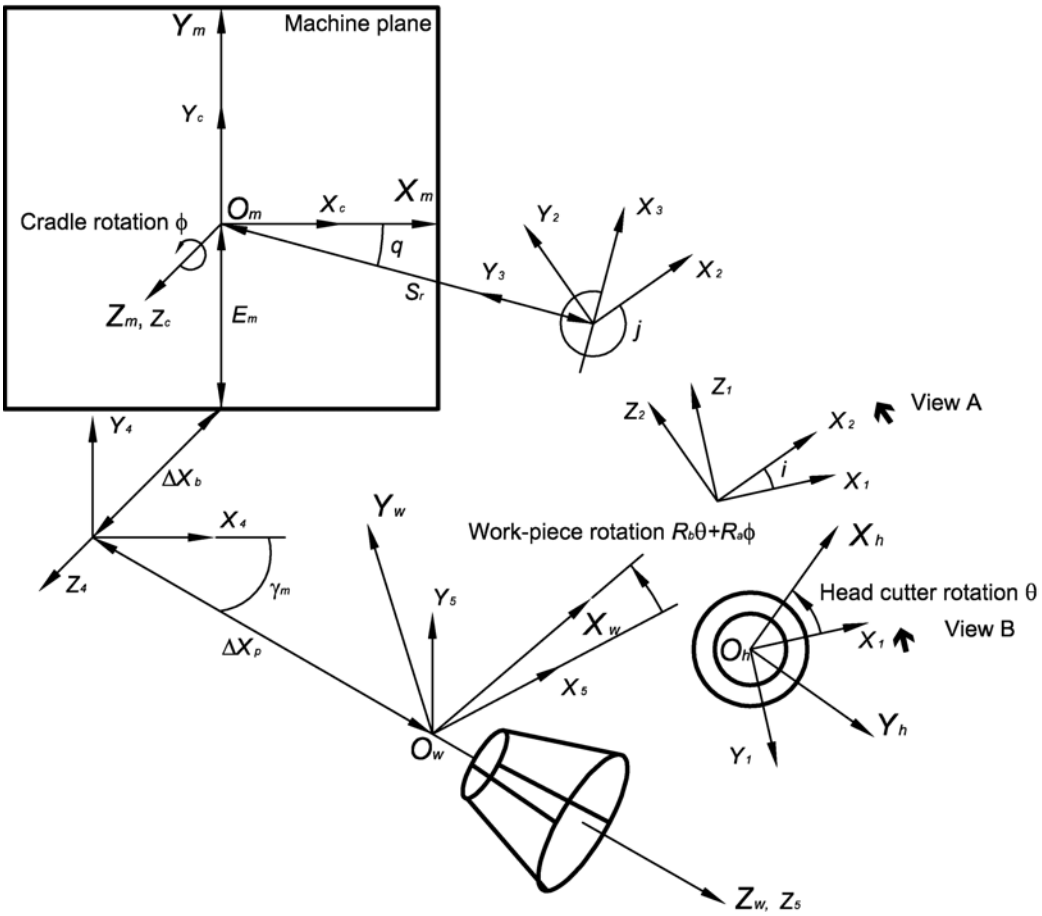

Figure 5. Sketch of a cutting machine set up for manufacturing a generated FH gear drive.

By properly computing the matrices for coordinates transformations (see Appendix A), the cutting edge representation in the system S_w is derived:

$$\boldsymbol{r}_w(\theta,\phi,s) = \boldsymbol{M}_{w5}\boldsymbol{M}_{54}\boldsymbol{M}_{4m}\boldsymbol{M}_{mc}\boldsymbol{M}_{c3}\boldsymbol{M}_{32}\boldsymbol{M}_{21}\boldsymbol{M}_{1h}\boldsymbol{r}_h(s) \qquad (3)$$

As well known, Equation (3) represents a family of surfaces; with the aim to compute tooth surfaces, one has to search for the envelope of this family by solving equation of meshing:

$$\left(\frac{\partial}{\partial s}\boldsymbol{r}_w(\theta,\phi,s)\times\frac{\partial}{\partial\theta}\boldsymbol{r}_w(\theta,\phi,s)\right)\bullet\frac{\partial}{\partial\phi}\boldsymbol{r}_w(\theta,\phi,s)=0 \qquad (4)$$

By using values of θ, ϕ and *s* that satisfy Eq. (3), Eq. (4) and the tooth geometric boundaries, a surface for each section of the blade is generated[*]. For example, considering previously discussed blade, four surfaces, corresponding to the four blade parts (bottom, fillet, Toprem® and curved blade), are obtained.

In order to compute final tooth surfaces, it is necessary to handle properly these four surfaces. Due to the severe analytical complexity of these equations, a convenient way to accomplish this step is to slice the tooth by means of several cross sections and to compute numerically the tooth profiles belonging to these cross sections; in other words, by solving a non-linear problem, four profiles cut by the four parts of the blades and belonging to the selected cross section are firstly calculated. Then, these four profiles have to be correctly merged. If non-generated cutting process is simulated, the four parts of profile are very regular and its composition is a trivial task (Figure 6, on the left). If a generated pinion is considered, the enveloping process induces a more intricate profile (Figure 6, on the right): discontinuities and intersections between the four

[*] When representation of a non-generated gear is needed, cradle rotation ϕ is null and tooth surfaces are computed only by means of Eq. (3) that becomes a function of two parameters (θ and *s*).

sections of profile are usually detected. In particular fillet can intersects active flank and undercutting takes place. The proposed model is able, by means of numerical procedures based on simple vector properties [14], to detect all these intersections, to eliminate all that points not belonging to the real profile and, using the remaining points, to compute the final tooth profile.

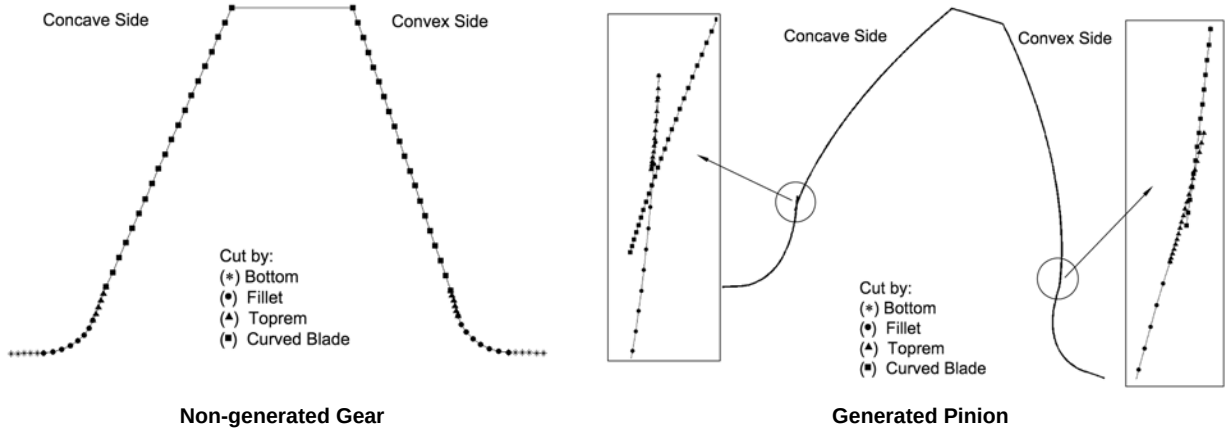

Figure 6. Example of tooth sections computed by the proposed model.

4. Computerized Analysis of Face Hobbed Hypoid Gear Drives

In this section, by means of the proposed model tooth surface representation of a real case will be derived and the results accurately validated; then, by simulating the meshing, performance analysis, including contact analysis under light and heavy loads and stress analysis, will be carried out.

A FH hypoid gear drive belonging to a truck differential system is considered. Table 1 reports the main geometric data of this example; the pair carries a 44 teeth gear and a 15 teeth pinion.

Table 1. Geometric data of the example case.

			Pinion	Gear
Module	[1/mm]	m	5.11	
Shaft Angle	[°]	Σ	90	
Number of Teeth		N	15	44
Mean Spiral Angle	[°]	ψ	43.00	28.90
Hand of Spiral			LH	RH
Face Width	[mm]	F	41.43	38.00
Outer Cone Distance	[mm]	A_o	106.40	126.10
Pitch Angle	[°]	γ	26.88	62.41
Addendum	[mm]	a	5.09	2.96
Dedendum	[mm]	b	3.91	6.04

The gear member is Formate® while the pinion is obtained using generation motion; for the pinion, tilt and swivel mechanisms are employed. Regarding cutting tools, Gleason Tri-ac® head cutter with 13 blade groups is used; the gear is cut by curved blades, the pinion by curved blades with Toprem®. For both the members, nominal blade radius of curvature is equal to 762 mm.

4.1. Tooth Surface Representation

By means of the algorithms proposed in Paragraph 3, tooth surface representation of studied gear drive has been computed. In Figure 7.a, the results obtained for the gear member are shown; as expected, the non-generated member presents tooth profiles which are very regular and similar to the cutting edge shape. Figure 7.b reports the surfaces obtained for the pinion; in this case, the enveloping process induces more complicated tooth geometry which requires a wider discussion. Consider Figure 8, where the results obtained for two characteristic cross sections of the studied pinion are reported. As often it happens in uniform depth tooth, toe-section (Fig. 8.a, above) shows undercutting (on concave side) and very sharp topland. The different pressure angle value between inner blade and outer blade induces a concave profile different from the convex one. Moreover, neither of the sections has tooth height equal to the nominal one (NTH); in particular the heel section concave side height is about 5.5% higher than the nominal one (Fig. 8.b, above). Pictures of the real tooth (Fig. 8.a and 8.b, below) make clear that the proposed mathematical model is able to capture accurately the tooth shape.

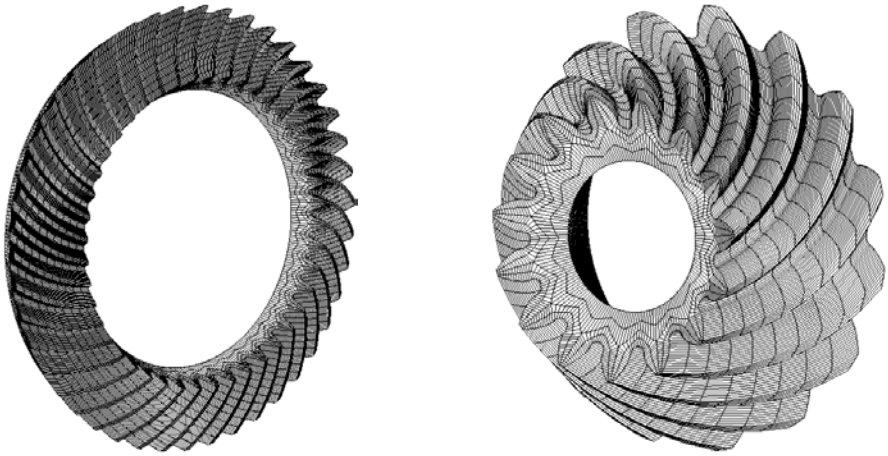

(a) (b)

Figure 7. Tooth surface representation obtained by means of the proposed model.

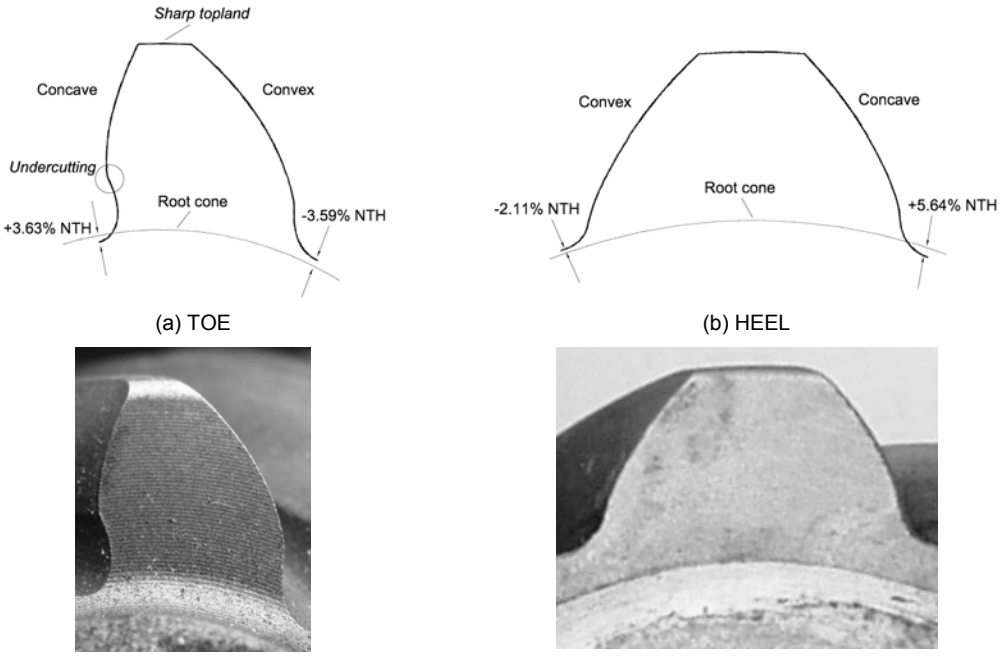

(a) TOE (b) HEEL

Figure 8. Pinion cross-sections obtained by means of the proposed model compared with the real tooth.

In order to validate quantitatively these results, the obtained surfaces are compared with the ones calculated by software Gleason T801Z0® which is considered a reliable reference. By means of the two theoretical models, coordinates of the concave and convex active flanks for both of gear and pinion are computed; discrepancies between the two surfaces are evaluated as normal deviation of homologue points over a grid containing 15 points along lead and 9 points along tooth profile. For both the pinion and the gear, the normal deviation between the two models has been revealed very small (mean value below 0.1 μm) and uniformly distributed over the flank; thus, the mathematical model proposed in this paper allows to describe accurately FH tooth geometry.

4.2. Simulation of Meshing: Contact and Stress Analysis

The gear tooth surfaces representation which has been previously computed and validated, it has been employed as input for an advanced contact solver which combines the Boussinesq theory (for solving the contact problem) and traditional finite

element method (for computation of gross deflections associated with tooth bending) [10-11]. This approach allows to build an accurate numerical model with a relative coarse mesh and to carry out very efficiently contact analysis and stress calculation.

Figure 9 shows the settings of the model prepared for these analyses. Gear meshing is studied in the fixed reference frame S_g that is rigidly connected to the housing; the system $S_{f,1}$ and $S_{f,2}$ are defined in order to take into account the relative position of pinion and of gear with respect of the system S_g; in this way, it is also simple to introduce the installment errors (ΔE, ΔP, ΔG and $\Delta\Gamma$).

According to Figure 9 (on the right), pinion rotation is considered by means of system $S_{w,1}$ which is rigidly connected to the pinion; as mentioned, this frame has been also used to compute tooth surface equations. Gear rotation is similarly handled.

Boundaries conditions are placed according to a simplified approach, already seen in the literature [4]: the internal pinion rim is constrained to 5 degrees of freedom and the torque is imposed; the internal gear rim is fully constrained.

When drive side is analyzed, contacting surfaces are pinion concave/gear convex, the contrary for coast side condition. The contact is simulated as frictionless.

The material is defined as steel with the properties of Young's modulus E = 210000 N/mm^2 and the Poisson's ratio v = 0.3.

The analyses carried out in this paper are static: in a given instant of cycle of meshing, pinion and gear are rotated to an angle where they are in contact in a single point and the contact is solved. It follows that, in order to study the whole cycle of meshing, many instants have been analyzed.

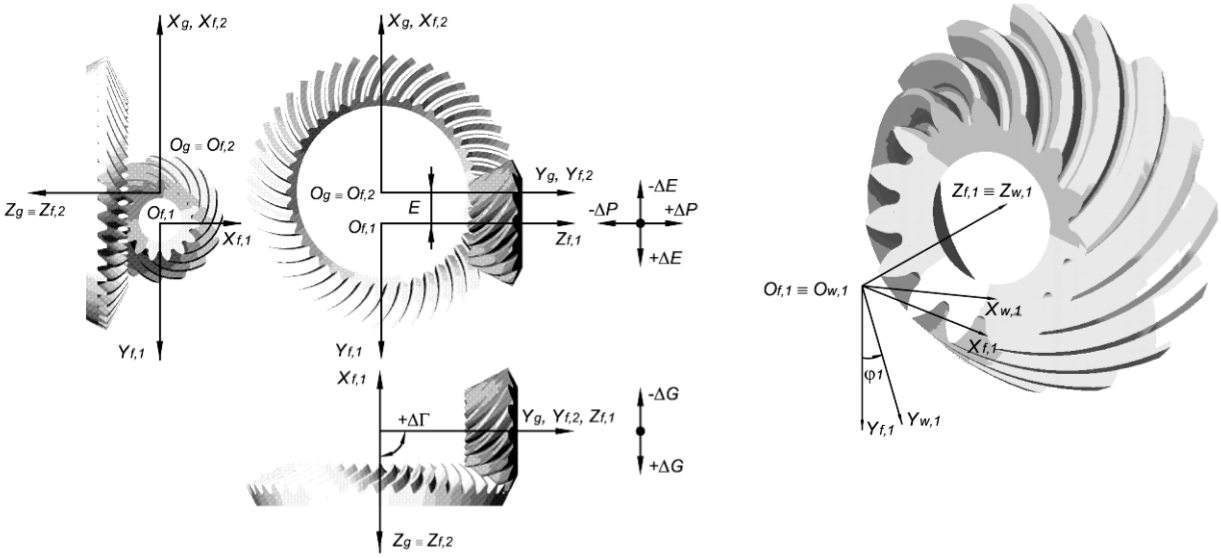

Figure 9. Settings of the numerical model used for performance analysis.

4.2.1. Tooth Contact Analysis

As known [15], TCA theory is based on the assumption that the applied torque is null and the gear teeth are rigid; this approach is implemented in most of the proprietary software (as example the TCA module of Gleason T2000®). In this paper, due to the fact that the contact solver employees finite element method, a torque, though very light (0.0001 Nm), has to be applied; moreover the teeth show the stiffness which is deriving from the characteristics of geometry and material. Table 2 reports the conditions analyzed in this paper.

Table 2 – TCA conditions simulated in this paper.

ID Case	Side	Contact Position	ΔE [mm]	ΔP [mm]	Torque [Nm]
TCA.1	Drive	Toe	0.254	-0.102	~ 0
TCA.2	Drive	Mean	0	0	~ 0
TCA.3	Drive	Heel	-0.508	0.280	~ 0
TCA.4	Coast	Toe	-0.254	0.051	~ 0
TCA.5	Coast	Mean	0	0	~ 0
TCA.6	Coast	Heel	0.508	-0.254	~ 0

For drive and coast side, toe, mean and heel contact position have been considered. Installment errors for toe and heel position are computed considering a distance from the mean point of 0.25*F* respectively towards the toe and towards the heel.

In Table 3, the results obtained by running analysis by means of the proposed model (named HYFH) are illustrated; for each analyzed case, contact pattern and transmission error (TE) are reported. This latter parameter has been defined as the difference in the angular displacement of the gear member from the theoretically exact position based on the ratio of the numbers of teeth, at different pinion angular rotation:

$$\mathrm{TE} = \Delta\varphi_2 = \varphi_2 - \frac{N_1}{N_2}\varphi_1 \tag{5}$$

Path of contact (i.e. white points superimposed to contact pattern) is oblique and remains correctly in the tooth boundaries. Transmission error shows the typical negative parabolic shape according to the examples in the literature [16].

Table 3 summarizes also Peak to Peak transmission error (PPTE), which gives an idea of the gear noise level; these results are compared with the ones calculated by TCA module of Gleason T2000®; as evident, the agreement is quite satisfactory.

Table 3 – Results computed by HYFH in TCA condition compared with the ones calculated by T2000®.

ID Case	Gear Contact Pattern (HYFH)	Transmission Error (HYFH)	PPTE (HYFH) [μrad]	PPTE (T2000) [μrad]	ΔPPTE [%]
	Toe Heel				
TCA.1		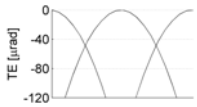	49	52	-5.8
TCA.2		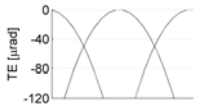	51	54	-4.9
TCA.3		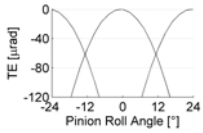	62	63	-1.9
	Heel Toe				
TCA.4		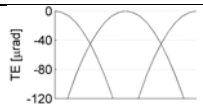	45	47	-4.7
TCA.5		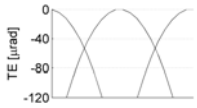	53	57	-6.7
TCA.6		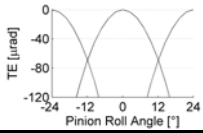	70	76	-7.9

4.2.2. Loaded Tooth Contact Analysis

Aim of LTCA is to study contact pattern and motion error in loaded state, allowing a better understanding of the real gear drive performance [17]. By means of the proposed model (named HYFH), the truck transmission has been analyzed to 7 values of torque which are applied in normal service condition (Table 4); drive side at mean contact point is considered.

In Table 5 the results regarding contact analysis are summarized.

Table 4 - LTCA developed in this paper.

ID Case	Side	Contact Position	Δ*E* [mm]	Δ*P* [mm]	Torque [Nm]
LTCA.1	Drive	Mean	0	0	940
LTCA.2	Drive	Mean	0	0	670
LTCA.3	Drive	Mean	0	0	500
LTCA.4	Drive	Mean	0	0	335
LTCA.5	Drive	Mean	0	0	250
LTCA.6	Drive	Mean	0	0	170
LTCA.7	Drive	Mean	0	0	100

Table 5 – Contact pattern and contact pressure computed by HYFH in LTCA conditions.

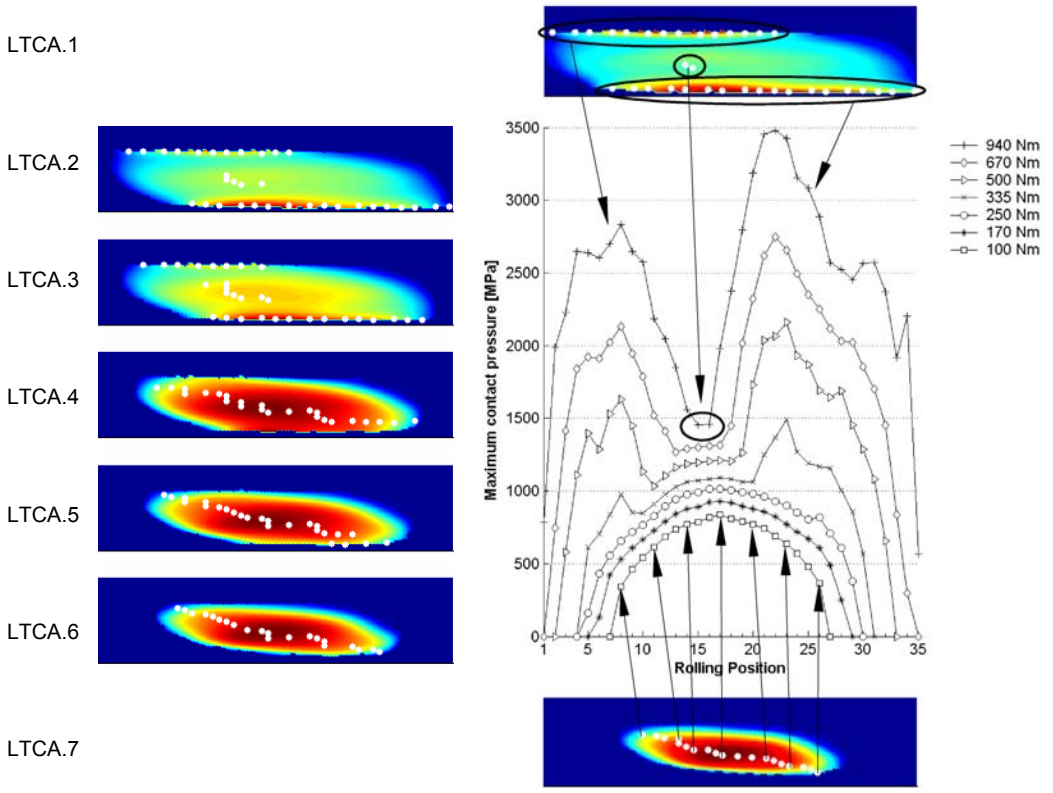

For each applied torque value, path of contact (i.e. white points corresponding to the point in the tooth where, in a given instant of meshing, maximum value of contact pressure is reached) superimposed to the contact pattern (i.e. envelope of contact pressure) is shown. The diagram on the right reports, for each values of applied torque, maximum contact pressure value at successive positions of roll corresponding to previously mentioned white points. Observing these results, it is possible to note that, as load increases, the contact pattern enlarges until, for torque above to 250 Nm, edge contact with pressure peaks happens. Actually, most of these peaks are flattened due to material plasticity or to corner smoothing induced by wear.

Considering motion transmission, in Figure 10 (on the left), Harris map (i.e. plotting, for each applied torque, of transmission error versus two pinion angular pitches) superimposed to TCA results (continuous lines) are reported. On the right of Figure 10, PPTE and load sharing (i.e. Actual Total Contact Ratio $\varepsilon_{\gamma,act}$) trends versus applied torque are summarized as well. These diagrams makes evident that as load increases, TE curve flattens shifting the phase; this evidence is due to the meshing stiffness variation as the number of teeth in contact changes. At the torque value equal to 335 Nm, where the load is shared between 2 and 3, almost uniform motion is achieved (PPTE equal to 8 μrad); this evidence agrees with Welbourne's work [18] where he points out that there is an optimum for PPTE value corresponding to minimum noise condition. For torque values above 500 Nm, motion curve changes again because now the load is shared between 3 and 4 teeth; in this case, the difference in stiffness for 4 versus 3 teeth is less than for 3 versus 2 so the smoothing of the motion curve occurs at a slower rate.

By comparing all these results with the ones calculated by the LTCA module of Gleason T2000®, it is possible to conclude that reference software computes a stiffer meshing. In fact, Fig. 11 (on the left) makes clear that Gleason® code shares the load on a smaller number of teeth and consequently calculates different values of PPTE; moreover (Fig. 11, on the right), maximum contact pressures are lower and edge contact condition is never achieved due to the smaller size of contact pattern.

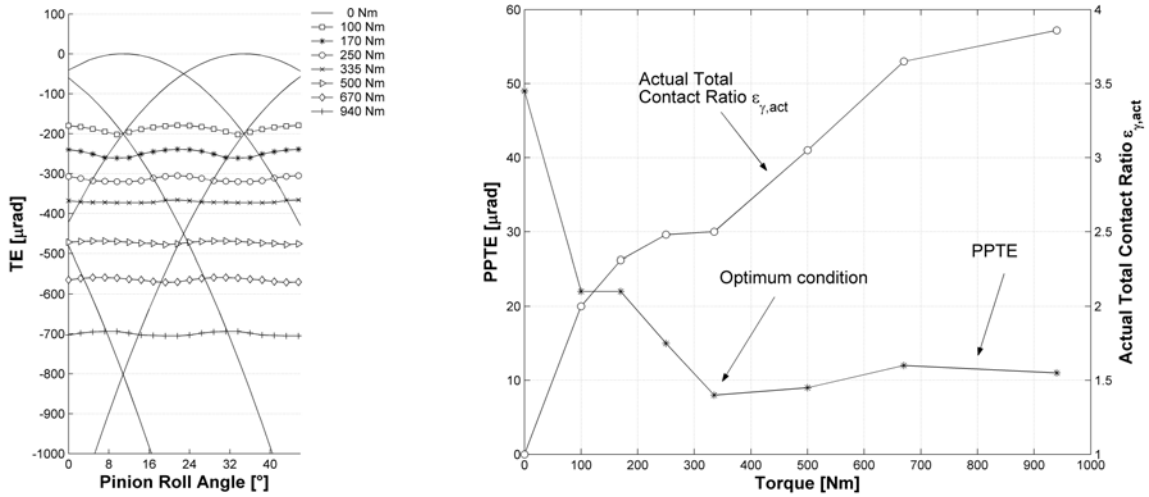

Figure 10. Harris map and PPTE-Actual Total Contact Ratio ε_γ trends computed by HYFH.

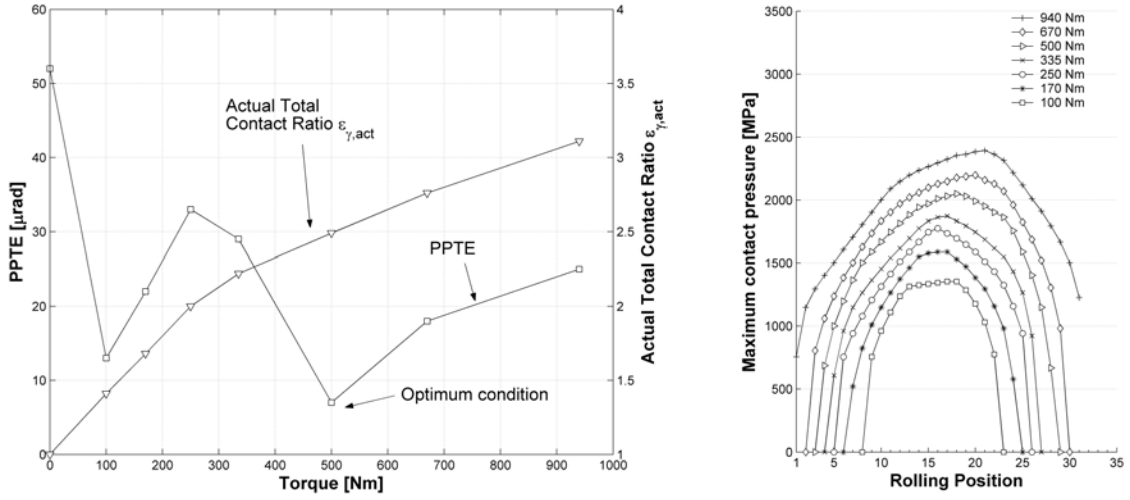

Figure 11. Results (PPTE-Actual Total Contact Ratio ε_γ and contact pressure) computed by T2000®.

It is reasonable to attribute these discrepancies to the different analysis approach which is adopted by the two codes. As shown, the one used by HYFH is based on a combination of Boussinesq theory with FE method and allows to build a numerical model able to describe accurately the complex tooth geometry; on the contrary, Gleason® code follows an approximate method assuming the gear tooth as a cantilever beam for calculation of tooth deflection [17]. According to these considerations, it seems that the results obtained by means of the proposed model can be considered more realistic and reliable.

4.2.3 Stress Calculation

By means of the proposed model it is easy to compute stress distribution on the teeth.

Referring to the example case, for each values of applied torque, bending stress during the whole meshing cycle has been monitored. In the fillet region, it has been searched for the coordinates of the point on the pinion and on the gear, where maximum value of Von Mises stress has been taken place; when, as in this case, drive condition and mean contact point is considered, this point is usually located in the middle of face width. Here, the trend of Von Mises stress versus time has been plotted. Figure 12 shows obtained results; it is evident that the gear drive is properly design with the aim to uniformly balance stress on the gear member and on the pinion; moreover these graphs allow to study fatigue loading condition of gear drive.

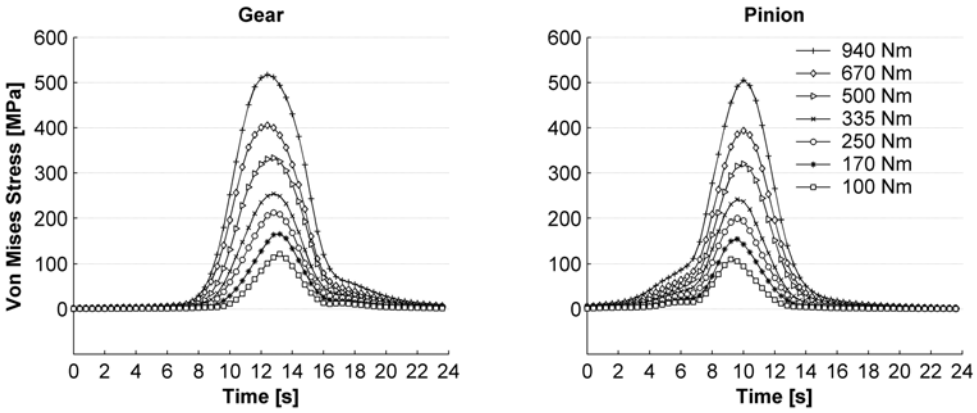

Figure 12. Bending stress versus time computed by means of proposed model.

5. Conclusions

In this paper an accurate tool for computerized design of face hobbed hypoid gears has been presented.

In order to accomplish this goal, firstly, a mathematical model able to compute detailed gear tooth surface representation starting from cutting process has been developed. Gleason Tri-Ac® head cutter has been considered and complex blade configurations (curved blade with Toprem®) has been studied; cutting process with or without generation motion can be handled. The proposed model allows to get a fine tooth surface description; it is also able to efficiently deal with undercutting occurrence. With the aim to validate the model, gear tooth surfaces of a real case (truck differential system) have been computed and the results compared with the ones calculated by a reference software obtaining good agreement.

Then, these tooth surfaces have been provided to a powerful contact solver and performance analysis has been developed. The truck transmission has been studied, monitoring contact pattern and transmission error, in TCA condition at several contact positions. After that, in order to examine thoroughly gear drive performance in the real service conditions, LTCA has been developed; the influence of variation of the applied torque value on tooth contact pattern, on transmission error and on load sharing has been accurately analyzed. Contact pressure on the active flank and stress distribution in the fillet region has been monitored as well.

The obtained results have been compared with the ones calculated by a reference software. In TCA condition a good agreement has been achieved; in LTCA condition, where the stiffness of the teeth plays an important role, some discrepancies have been noted. The cause of these evidences has to be searched mainly in the different approach used in the solution of the problem; in particular, the two codes compute tooth deflection in a very different way.

These considerations allow to conclude that the model presented in the paper can be considered a reliable numerical tool for studying face hobbed hypoid gear drive; in order to make more realistic the model, studies are foregoing for the whole differential system simulation which will allow to correctly consider also the deflection due to the load.

References

[1] D.W. DUDLEY, D.P. TOWNSEND, *Dudley's Gear Handbook,* McGraw-Hill Inc., New York 1992.

[2] H.J. STADTFELD, *Advanced Bevel Gear Technology*, The Gleason Works, Rochester, NY, 2000.

[3] F.L. LITVIN, Y. GUTMAN, *Methods of Synthesis and Analysis for Hypoid Gear-Drives of "Formate" and "Helixform"*, Part 1, 2, and 3, ASME J. Mech. Des. 103 (1) (1981) 83-113.

[4] J. ARGYRIS, A. FUENTES, F.L. LITVIN, *Computerized Integrated Approach for Design and Stress Analysis of Spiral Bevel Gears*, Comput. Methods Appl. Mech. Engrg, 191 (2002) 1057-1095.

[5] C. GOSSELIN, T. GUERTIN, D. REMOND, Y. JEAN, *Simulation and Experimental Measurement of the Transmission Error of Real Hypoid Gears Under Load*, ASME J. Mech. Des. 122 (2000) 109-122.

[6] F.L. LITVIN, A. FUENTES, Q. FAN, R.F. HANDSCHUH, *Computerized Design, Simulation of Meshing, and Contact and Stress Analysis of Face-Milled Formate*

Generated Spiral Bevel Gears, Mech. Mach. Theory 37 (2002) 441-459.

[7] F.L. LITVIN, W.S. CHAING, C. KUAN, M. LUNDY, W.J. TSUNG, *Generation and Geometry of Hypoid Gear-Member with Face-Hobbed Teeth of Uniform Depth*, Int. J. Mach. Tools Manufact. 31 (2) (1991) 167-181.

[8] Z.H. FONG, *Mathematical Model of Universal Hypoid Generator with Supplemental Kinematic Flank Correction Motions*, ASME J. Mech. Des. 122 (2000) 136-142.

[9] M. VIMERCATI, *Mathematical Model for Tooth Surfaces Representation of Face-Hobbed Hypoid Gears*, submitted for publication to Comput. Methods Appl. Mech. Engrg.

[10] S.M. VIJAYAKAR, *Calyx Users Manual,* Advanced Numerical Solution, Hilliard, OH, 2003.

[11] S.M. VIJAYAKAR, *A Combined Surface Integral and Finite Element Solution for a Three-Dimensional Contact Problem*, Int. J. Numer. Methods Eng. 31 (1991) 525–545.

[12] H.J. STADTFELD, *The New Way of Manufacturing Bevel and Hypoid Gears in a Continuous Process*, AGMA Fall Techical Meeting, 1996.

[13] F.L. LITVIN, *Gear Geometry and Applied Theory*, Prentice Hall, Englewood Cliffs, NJ, 1994.

[14] S.M. VIJAYAKAR, B. SARKAR, D.R. HOUSER, *Gear tooth profile determination from arbitrary rack geometry*, AGMA Fall Techical Meeting, 1987.

[15] *Understanding Tooth Contact Analysis*, Gleason Works Publication, SD3139, 1978

[16] F.L. LITVIN, L. FLONG-TAO, *Generation and Tooth Contact Analysis of Spiral Bevel Gears with Predesigned Parabolic Functions of Transmissions Errors*, NASA Report 4259, 1989.

[17] T.J. KRENZER, *Tooth Contact Analysis of Spiral Bevel and Hypoid Gears Under Load*, The Gleason Works, Rochester, NY, 1981.

[18] D.B. WELBOURN, *Gear Errors and Their Resultant Noise Spectra*, Proceedings Institute of Mechanical Engineers, 1969-70, Vol. 184, Pt. 30.

Appendix A
Matrices describing cutting process

1) Transformation $S_h \rightarrow S_1$: Head cutter rotation

$$\boldsymbol{M}_{1h} = \begin{bmatrix} \cos\theta & \sin\theta & 0 & 0 \\ -\sin\theta & \cos\theta & 0 & 0 \\ 0 & 0 & 1 & 0 \\ 0 & 0 & 0 & 1 \end{bmatrix} \tag{1}$$

2) Transformation $S_1 \rightarrow S_2$: Tilt angle

$$\boldsymbol{M}_{21} = \begin{bmatrix} \cos i & 0 & \sin i & 0 \\ 0 & 1 & 0 & 0 \\ -\sin i & 0 & \cos i & 0 \\ 0 & 0 & 0 & 1 \end{bmatrix} \tag{2}$$

3) Transformation $S_2 \rightarrow S_3$: Swivel angle

$$\boldsymbol{M}_{32} = \begin{bmatrix} \cos j & -\sin j & 0 & 0 \\ +\sin j & \cos j & 0 & 0 \\ 0 & 0 & 1 & 0 \\ 0 & 0 & 0 & 1 \end{bmatrix} \tag{3}$$

4) Transformation $S_3 \rightarrow S_c$: Head cutter settings

$$\boldsymbol{M}_{c3} = \begin{bmatrix} \cos(\pi/2-q) & -\sin(\pi/2-q) & 0 & 0 \\ +\sin(\pi/2-q) & \cos(\pi/2-q) & 0 & -S_r \\ 0 & 0 & 1 & 0 \\ 0 & 0 & 0 & 1 \end{bmatrix} \tag{4}$$

5) Transformation $S_c \rightarrow S_m$: Cradle rotation

$$\boldsymbol{M}_{mc} = \begin{bmatrix} \cos\phi & -\sin\phi & 0 & 0 \\ \sin\phi & \cos\phi & 0 & 0 \\ 0 & 0 & 1 & 0 \\ 0 & 0 & 0 & 1 \end{bmatrix} \tag{5}$$

6) Transformation $S_m \rightarrow S_4$: Work-piece settings

$$\boldsymbol{M}_{4m} = \begin{bmatrix} 1 & 0 & 0 & 0 \\ 0 & 1 & 0 & +E_m \\ 0 & 0 & 1 & -\Delta X_b \\ 0 & 0 & 0 & 1 \end{bmatrix} \tag{6}$$

7) Transformation $S_4 \rightarrow S_5$: Work-piece settings

$$\boldsymbol{M}_{54} = \begin{bmatrix} \cos(\pi/2-\gamma_m) & \sin(\pi/2-\gamma_m) & 0 & 0 \\ -\sin(\pi/2-\gamma_m) & \cos(\pi/2-\gamma_m) & 0 & 0 \\ 0 & 0 & 1 & -\Delta X_b \\ 0 & 0 & 0 & 1 \end{bmatrix} \tag{7}$$

8) Transformation $S_5 \rightarrow S_w$: Work-piece rotation

$$\boldsymbol{M}_{w5} = \begin{bmatrix} \cos(R_b\theta + R_a\phi) & \sin(R_b\theta + R_a\phi) & 0 & 0 \\ -\sin(R_b\theta + R_a\phi) & \cos(R_b\theta + R_a\phi) & 0 & 0 \\ 0 & 0 & 1 & 0 \\ 0 & 0 & 0 & 1 \end{bmatrix} \tag{8}$$